RADIO SCIENCE, VOL. 44, RS2S91, doi:10.1029/2007RS003821, 2009

Truncation effects in a semi-infinite periodic array of thin strips: A discrete Wiener-Hopf formulation

F. Capolino[1] and M. Albani[2]

Received 28 December 2007; revised 18 April 2008; accepted 29 January 2009; published 10 April 2009.

[1] A rigorous solution for the current induced on a semi-infinite array of narrow metallic strips is obtained using the Wiener-Hopf factorization method in the Z-transformed domain. The method can be applied to arrays with fixed current shape on each element (e.g, single mode elements), and shows rigorously the physics of waves associated to truncated periodic structures. The solution is obtained via a rigorous factorization, that is improved by using a closed form result based on an approximated factorization. The current on the truncated array is rigorously represented as the sum of the current pertaining to the infinite array plus a contribution induced by the truncation of the array. Asymptotics shows that the truncation-induced current contribution has a diffractive behavior decaying algebraically with the element number, away from the truncation. Uniform asymptotics shows that this diffractive current is effectively represented in terms of Fresnel functions, permitting also a closed form representation in proximity of and at transverse inward resonance, i.e., when a grazing grating lobe points toward the array. Illustrative examples and comparisons with a method of moment solution show the accuracy of our results.

Citation: Capolino, F., and M. Albani (2009), Truncation effects in a semi-infinite periodic array of thin strips: A discrete Wiener-Hopf formulation, *Radio Sci.*, *44*, RS2S91, doi:10.1029/2007RS003821.

1. Introduction

[2] Wave characterization and modeling for arrays with a large number of elements have been subject of various studies in the recent years. Assuming the structure as infinite when using a full-wave model, though simple and efficient it may not be satisfactory when array-truncation effects are relevant. Owing to the localization of the truncation-induced diffracted waves for large arrays, many physical insights of the wave processes can be extracted from a canonical problem such as a semi-infinite array of impressed electric line sources or dipoles [*Kildal*, 1984; *Carin and Felsen*, 1993; *Felsen and Carin*, 1994; *Capolino et al.*, 1998, 2000a, 2000b]. In the present paper, we deal with the exact analysis of a semi-infinite array of narrow perfectly conducting strips illuminated by a plane wave. The same structure was analyzed by *Carin and Felsen* [1993] with a hybrid (ray) (Floquet) (MoM) efficient formulation; however, truncation field effects were accounted for by using a Kirchhoff approximation; i.e., the current on the strips were assumed as those of the array assumed as infinite. Successively, truncation effects were numerically refined by *Neto et al.* [2000a, 2000b], *Çivi et al.* [2000], and *Craeye et al.* [2004] using a MoM with basis functions shaped as truncation-induced diffracted fields.

[3] Here, the problem of a semi-infinite array of narrow perfectly conducting strips is solved rigorously by using a discrete Wiener-Hopf technique which has the advantage of being both exact and analytically explicit. This electromagnetic problem reduces to the scalar case where the Dirichlet boundary condition is imposed on the strips. The Wiener-Hopf method is a well established technique. Electromagnetic or acoustic problems usually involve branch point singularities, and the general formalism is given by *Noble* [1958], *Kobayashi* [1990], and *Jones* [1964] where the method was applied in the classical spectral wave number along a cartesian axis. In other fields, like digital signal processing or control theory, the Wiener-Hopf method is combined with the Z transform of successions of samples but they do not deal with branch point singularities because the spectral

[1]Department of Electrical Engineering and Computer Science, University of California, Irvine, California, USA.
[2]Department of Information Engineering, University of Siena, Siena, Italy.

0048-6604/09/2007RS003821$11.00

kernels to be factorized are usually rational. There are a few papers where the Wiener-Hopf method was applied in the Z-transformed domain to solve diffraction problems with a discrete set of scatterers, thus involving branch points singularities [*Fel'd*, 1958; *Hills and Karp*, 1965; *Koughnett*, 1970; *Wasylkiwskyj*, 1973; *Linton and Martin*, 2004].

[4] In the work of *Fel'd* [1958] the problem was formulated for a semi-infinite array of cylinders (as in the work of *Hills and Karp* [1965]) by using the Z transform and the factorization method [*Fel'd*, 1958, equation (17)], but, as the authors themselves admit, their formulation leads to complicated integrals and the problem is instead solved by a variational principle.

[5] The discrete Wiener-Hopf technique was applied in the remarkable paper by *Hills and Karp* [1965] to treat a semi-infinite grating of small cylinders under the hypothesis of electrically large interelement spacing ($d \gg \lambda$, with d the array period and λ the free space wavelength).

[6] In the work of *Koughnett* [1970] a beautiful analysis in terms of Z-transformed quantities was given for an array of dipole antennas, and a formal solution was provided as the sum of factorized terms that, however, were not explicitly evaluated. Only the case with mutual couplings set to zero after a certain distance was numerically solved. In this way the difficulty arising from treating branch point singularities was avoided. In general, truncation effects vanish after a certain number of array elements but there are important cases where truncation effects may extend over a large portion of the array; e.g., when the period is much smaller than the wavelength or when near "resonance" conditions occur.

[7] In the work of *Wasylkiwskyj* [1973] the Z domain Wiener-Hopf method was extensively explained but the factorization was not performed in the way shown in this paper, though various formulas and simplifications were there provided. Furthermore, the aim of that paper was about showing truncation effects in input parameters for arrays of minimum-scattering dipole antennas [*Wasylkiwskyj and Kahn*, 1970], and not about diffractive effects arising form the array truncation. No high-frequency concepts were discussed by *Wasylkiwskyj* [1973].

[8] In the work of *Nishimoto and Ikuno* [1999] a strip grating as in this paper was analyzed, in contrast to gratings of small cylinders as in the works of *Fel'd* [1958] and *Hills and Karp* [1965]. There, the problem was not solved with the Wiener-Hopf method but some interesting properties of the diffracted current were shown.

[9] In the work of *Linton and Martin* [2004] the Z domain Wiener-Hopf method was shown to solve semi-infinite arrays made of strips and of cylindrical scatterers, with Dirichlet boundary condition (soft case). There, diffraction effects were extensively discussed, but the analysis is different than that in our paper though there are similarities.

[10] In summary in the works of *Fel'd* [1958], *Koughnett* [1970], and *Wasylkiwskyj* [1973], no diffraction effects and high-frequency concepts are emphasized as in the works of *Hills and Karp* [1965], *Nishimoto and Ikuno* [1999], *Linton and Martin* [2004], as well as in the present paper.

[11] In our formulation many new aspects are introduced compared to *Hills and Karp* [1965] and the other cited papers: (1) Arbitrary basis functions can be chosen to shape the current on the strip elements also permitting to treat both TE and TM polarizations, with respect to the direction of the strips, though in this paper we limit our analysis to the TM case; (2) The discrete Wiener-Hopf is implemented using a Z transform of the sampled distribution of currents. Here, the topology (critical points) of the z spectral plane is shown explicitly and discussed in details for a general semi-infinite structure. A complete correspondence between the discrete z spectral representation and the standard continuous plane wave k_x spectral wave number representation (the semi-infinite array is periodic along x) is established; (3) Solutions for any interelement spacing d as well as for the two limit cases of large ($d \gg \lambda$) and small ($d \ll \lambda$) d, compared to the wavelength λ, are automatically obtained from our formulation; (4) We provide an approximate factorization that is useful to approximate the currents on the strips and to numerically perform the exact factorization; (5) Asymptotics is performed via path deformation and SDP (steepest descent path) evaluation directly in the z plane (showing the correspondence to the k_x plane); (6) Asymptotic results are performed in a totally uniform fashion for the current on the strips. The diffracted current is found asymptotically as a sum of Floquet waves (solution for the infinite array) plus a diffracted current arising from the truncation of the array; (7) The general spreading factor $n^{-3/2}$ of the diffracted terms versus strip number n is obtained and discussed also showing its range of validity.

[12] Our solution is simple to use and offers a net physical insight into the behavior of the current in truncated periodic structures. We emphasize that our closed form solution can be directly applied to finite array of strips as long as the current diffracted at one edge of the array does not significantly couple with the other edge of the array.

2. Statement of the Problem

[13] The geometry of the semi-infinite array of conducting strips is shown in Figure 1, with definition of both cartesian and cylindrical coordinate systems centered at the array truncation. The period of the array is d

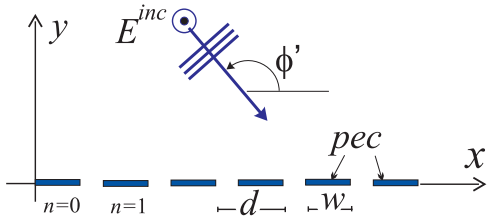

Figure 1. Semi-infinite array of conducting strips illuminated by a TM_z plane wave from a direction ϕ'. d is the array periodicity; w is the width of each strip. The plane wave illumination induce an array phasing $\exp(-jk_{x0}x)$ with $k_{x0} = -k \cos \phi'$.

and the strips have width w. For space limitation we analyze only the TM, with respect to z, case. The same treatment can be straightforwardly applied to the TE case. Also, the same method can be applied to semi-infinite arrays on media stratified along y and homogeneous along the x and z directions, so that the Green's function depends only on $x - x'$ and not separately on x and x'.

[14] The TM_z plane wave travels with phase speed c and arrives from a direction ϕ', as in Figure 1. The incident electric field on the array $E^{inc}(x') = \exp(-jk_{x0}x')$ is polarized along the z direction, has phasing $k_{x0} = -k \cos \phi'$ along the x direction, and $k = \omega/c$ is the free space wave number.

[15] The total current, along z, on each z-directed strip is represented using a single shape basis function that on the $n = 0$ strip is denoted by $h(x')$. Therefore, the current on a generic nth strip is represented as

$$J_n(x) = i_n h(x - nd), \tag{1}$$

where i_n is its weight and $h(x)$ differs from zero for $0 < x < w$. The weights i_n, $n = 0, 1, 2, \ldots$ represent the currents on the strips and are determined in the rest of this paper by solving the electric field integral equation with the Wiener-Hopf method.

3. Formulation

[16] The unknown current weights i_n are determined by imposing the vanishing of the total z-directed electric field component tangent to the conducting strips: $E^{sca}(x) + E^{inc}(x) = 0$ on the strips, i.e., for x such that $nd < x < nd + w$, with $n = 0, 1, 2, \ldots$ The term E^{sca} is the field scattered by all the currents $J_n(x)$. This condition is weighted on a generic mth strip by the test function $e(x - md)$. Thus the integral equation is equivalently expressed by the convolution

$$\sum_{n=0}^{\infty} k_{m-n} i_n = v_m. \tag{2}$$

Here, the impedance k_{m-n} represents the mutual coupling reaction integral between the current basis function $h(x - nd)$ on the nth strip and the the electric field test function $e(x - md)$ on the mth strip, whereas v_m is the voltage induced by the incident electric field on the mth strip. The impedance k_{m-n} is of Toeplitz type and given by

$$k_{m-n} = \int_0^w dx \int_0^w dx' h(x') g(x' + nd, x + md) e^*(x) \tag{3}$$

where $g(x, x') = g(x - x') = (k\zeta/4)\, H_0^{(2)}(k|x - x'|)$ is the free space Green's function, $H_0^{(2)}$ is the 0th order Hankel function of second kind, and * denotes complex conjugate, though often $e(x)$ is chosen to be real. The voltage v_m is given by

$$v_m = \int_{strip-m} E^{inc}(x)\, e^*(x - md) dx = V e^{-jk_{x0}md}, \tag{4}$$

with $V = \int_0^w e^{-jk_{x0}x}\, e^*(x) dx$. The weight i_n of the current basis function on each nth strip is found by solving (2). Owing to the discrete nature of the problem, we solve it in a Z-transformed domain. The convolution in (2) is expressed as the inverse Z transform (see Appendix A for definitions) of a product of Z-transformed quantities as

$$\frac{1}{2\pi j} \int_C K(z) I(z) z^{m-1} dz = V e^{-jmk_{x0}d} \tag{5}$$

where $K(z)$ and $I(z)$ are the Z transforms of the coupling impedance and current. Note that $i_n = 0$ for $n < 0$, and thus the Z transform $I(z)$ does not have singularities outside the unit circle in the complex z plane. In the following, $I(z)$ is found by using a factorization procedure, and the weight i_n of the current on the nth array element is found by the inverse Z transform. We can assume that the medium surrounding the grating has small vanishing losses, i.e., the wave number k has an arbitrary small negative imaginary part that is eventually removed.

[17] The Z transform $K(z)$ of the impedance k_{m-n}, defined in Appendix A, is found by using a k_x spectral (Fourier transform with respect to x) representation for the reaction integral (3) between basis and weight functions. This is achieved in the following steps. First, the impedance in (3) is rearranged by using the spectral plane wave representation of the free space Green's function

$$g(x - x') = \frac{k\zeta}{4\pi} \int_{-\infty}^{\infty} dk_x \frac{e^{-jk_x(x-x')}}{\sqrt{k^2 - k_x^2}}, \tag{6}$$

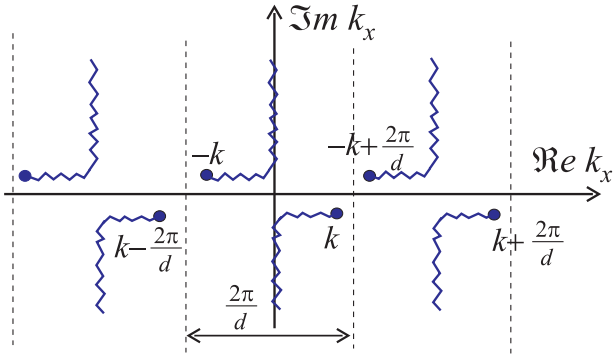

Figure 2. Complex k_x plane. Branches in the top half plane are located at $k_x = -k + 2\pi p/d$, whereas branches in the bottom half plane are in $k_x = k + 2\pi p/d$. The function $K(k_x)$ is periodic with period $2\pi/d$.

with $\Im m\{\sqrt{k^2 - k_x^2}\} \leq 0$ on the top Riemann sheet of the k_x complex plane. Equation (6) is inserted into (3), leading to

$$k_{m-n} = \frac{k\zeta}{4\pi} \int_{-\infty}^{\infty} dk_x \frac{H(k_x)E^*\left(k_x^*\right)}{\sqrt{k^2 - k_x^2}} e^{-jk_x d(m-n)} \tag{7}$$

with

$$H(k_x) = \int_0^w dx\, h(x)\, e^{jk_x x}$$
$$E(k_x) = \int_0^w dx\, e(x)\, e^{jk_x x} \tag{8}$$

denoting the Fourier transforms of basis and test functions. The Z transform $K(z)$ of the mutual impedance is thus found as

$$K(z) = \frac{k\zeta}{4\pi} \sum_{n=-\infty}^{\infty} z^{-n} \int_{-\infty}^{\infty} dk_x \frac{H(k_x)E^*\left(k_x^*\right)}{\sqrt{k^2 - k_x^2}} e^{-jk_x nd}. \tag{9}$$

The conformal mapping

$$z = e^{-jk'_x d}, \qquad k'_x = \frac{j}{d} \ln z \tag{10}$$

is used to establish a correspondence between the z and k'_x planes. The top (bottom) complex half k'_x plane is projected onto the region outside (inside) the unit circle of the complex z plane (see Figures 2 and 3). Once interchanged the order of integration and summation in (9), the Poisson formula $\sum_{n=-\infty}^{\infty} e^{-j\left(k_x - k'_x\right)nd} = \frac{2\pi}{d} \sum_{p=-\infty}^{\infty} \delta\left(k_x - k'_x - \frac{2\pi p}{d}\right)$ allows a closed form evaluation of the k_x integral, eventually yielding

$$K(z) = \frac{k\zeta}{2d} \sum_{p=-\infty}^{\infty} \left. \frac{H\left(k'_x + \frac{2\pi p}{d}\right)E^*\left(k_x'^* + \frac{2\pi p}{d}\right)}{\sqrt{k^2 - \left(k'_x + \frac{2\pi p}{d}\right)^2}} \right|_{k'_x = \frac{j}{d}\ln z} \tag{11}$$

The conformal mapping introduced in (10) introduces a branch point at $z = 0$ and a branch cut from $z = 0$ to $-\infty$ (see Figure 3). So the strip $-\pi/d < \Re e\ k'_x < \pi/d$ in the k'_x plane (see Figure 2) is mapped onto the top Riemann sheet of the complex z plane, and all the other strips bounded by dashed lines in Figure 2 are mapped onto top and bottom Riemann sheets of the z plane defined by (10). However, it is of crucial importance to note that the impedance expression (11) is periodic in k'_x with period $2\pi/d$. Therefore when it is transformed in the z domain via the mapping (10), all the Riemann sheets are equal and the branch cuts (between the infinite number of Riemann Sheets) from $z = 0$ to $-\infty$ are fictitious, i.e., there is no discontinuity on the z top Riemann sheet when crossing the branch cut. In the z plane $K(z)$ has two other branches that correspond to the branches in the strip $-\pi/d < \Re e\ k'_x < \pi/d$ in the complex k'_x plane. Using the mapping (10), the two branch points k and

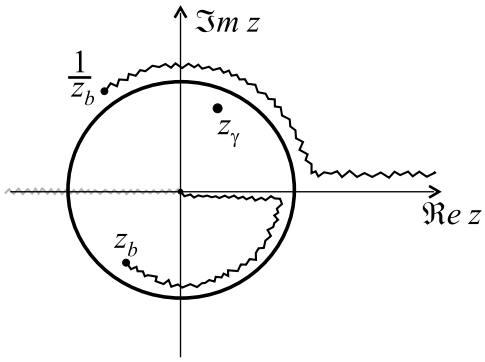

Figure 3. Complex Z plane. Unit circle; pole at $z_\gamma = \exp(-jk_{x0}d)$; branch points at $z_b = e^{-jkd}$ and $1/z_b$. The cut from $z = 0$ to $-\infty$ on the real axis, introduced by the mapping (10), is not present because of the periodicity of the function $K[\exp(-jk'_x d)]$.

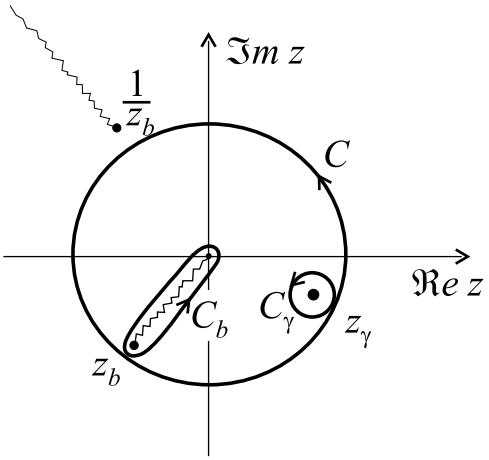

Figure 4. Contours of integration in the complex Z plane. $C \equiv$ unit circle; C_γ contour around the pole at z_γ; C_b contour around the branch cut connecting z_b to the origin. We have changed the branch cut definition with respect to Figure 3.

$-k$ in the k_x plane (see Figure 2) correspond to z_b and $1/z_b$ in the z plane (see Figure 3), with

$$z_b = e^{-jkd}. \tag{12}$$

[18] Owing to the assumed vanishing small losses, the branch points z_b and $1/z_b$ are located slightly inside and outside the unit circle, respectively. The branch cuts connecting k to $-j\infty$ and $-k$ to $j\infty$ in the k_x plane (Figure 2) are mapped onto the branch cuts connecting z_b to 0 and $1/z_b$ to ∞ in the z plane (Figure 3). The particular shape of the branch cuts is induced by that in the k_x plane given by $\Im m\{\sqrt{k^2 - k_x^2}\} = 0$. Since the basis and test functions $e(x)$ and $h(x)$ are defined onto limited domains $[0, w]$, their transforms $E(k'_x)$ and $H(k'_x)$ do not have singularities.

4. Wiener-Hopf Method

[19] The current i_n on a generic nth strip is found by solving (2). This is done by solving (5) by $I(z)$ and then calculating the currents i_n through the inverse Z transform defined in (40). Before proceeding further we note that $I(z)$ is analytic outside and on the unit circle ($|z| \geq 1$), to remark this property I will be also denoted by $I^+(z)$. Since (5) has to be verified for every $m > 0$, i.e., on every strip, the integrand in (5) must have the form

$$K(z)I^+(z) = V\frac{O^-(z)}{O^-(z_\gamma)}\frac{z}{z - z_\gamma} \tag{13}$$

in which

$$z_\gamma = e^{-jk_{x0}d} \tag{14}$$

and $O^-(z)$ is an unknown function analytic inside and on the unit circle ($|z| \leq 1$). The pole at $z = z_\gamma$ is located slightly inside the unit circle due to the small losses introduced ($k_{x0} = -k\cos\phi'$, with $\Im mk < 0$), see Figure 3. There are a number of excellent publications given in the Introduction dealing with the solution of an integral equation via the Wiener-Hopf factorization method. Here we follow the formalism in the work of *Born and Wolf* [1965] where the solution method is summarized in simple terms. The method requires a factorization

$$K(z) = K^+(z)K^-(z), \tag{15}$$

where $K^+(z)$ is free of zeros and singularities outside and on the unit circle, and $K^-(z)$ is free of zeros and singularities inside and on the unit circle. Such factorization is explicitly derived in Appendix B and in the next section. The only requirement we impose on such factorization is that $K^+(\infty)$ is finite and thus by definition $K^+(\infty) = k_0^+$. After insertion of such factorization (15) into (13), the latter is rewritten as

$$\frac{z - z_\gamma}{z}K^+(z)I^+(z) = \frac{O^-(z)}{O^-(z_\gamma)}\frac{V}{K^-(z)}. \tag{16}$$

The right hand side is now free of singularities inside and on the unite circle, and the left hand side is free of singularities outside and on the unit circle. Therefore, (16) is analytic in the whole complex z plane, thus it is a polynomial whose order is evaluated analyzing the behavior of the left hand side of (16) at $z = \infty$. Invoking the initial value theorem (see Appendix A) it can be seen that $I^+(\infty) = i_0$, whereas, by definition, $K^+(\infty) = k_0^+$. Therefore the left hand side of (16) is limited at $z = \infty$, and the polynomial is of zero order, i.e., it is simply a constant (for this reason a z was explicitly introduced at the numerator in the right hand side of (13)). The value of such a constant is determined evaluating the right hand side at $z = z_\gamma$ which leads to the solution $I(z)$ as

$$I(z) = I^+(z) = \frac{V}{K^+(z)K^-(z_\gamma)}\frac{z}{z - z_\gamma}. \tag{17}$$

[20] The currents i_n are obtained by using the inverse Z transform (40) of the result (17),

$$i_n = \frac{V}{2\pi j}\frac{1}{K^-(z_\gamma)}\int_C \frac{1}{K^+(z)}\frac{z^n}{z - z_\gamma}dz. \tag{18}$$

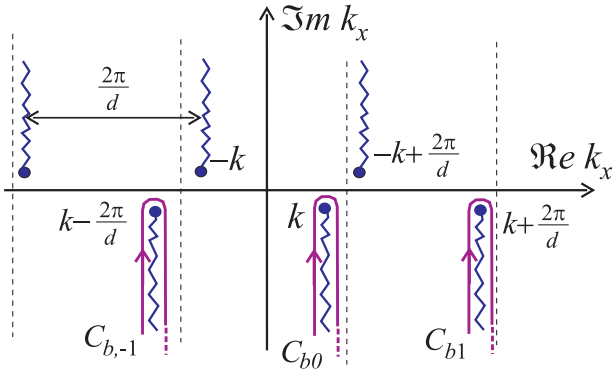

Figure 5. Mapping of the contour of integration C_b in Figure 4 onto the complex k_x plane.

[21] It may be convenient to use the equivalence $1/K^-(z_\gamma) = K^+(z_\gamma)/K(z_\gamma)$ in (18) and to keep inside the integral the ratio of factorized functions $K^+(z_\gamma)/K^+(z)$ which is independent of constant error factors introduced by using approximate factorizations (both $K^+(z)$ and $K^+(z_\gamma)$ would be affected by the same constant factor, and their ratio would be independent of it). Though for brevity we do not explicit it in the equations, this is indeed what we have used in the numerical evaluations of i_n.

[22] Note that for $z_\gamma \approx 1/z_b$, that occurs when $k_{x,p} = -k$ for some p, the solution vanishes as $\sqrt{1 - z_b z_\gamma} \approx 0$. This is denoted as the outward resonance case that corresponds to the pth Floquet harmonic propagating at grazing angle $\phi = 180°$, as discussed in section 8.3. The integral is evaluated deforming the integration path around the singularities inside the unit circle. These consist of a pole at $z = z_\gamma$, and a branch at $z = z_b$, as shown in Figure 3. In Figure 4 the branch cuts definition has been changed for convenience. We stress here that any particular definition does not affect the final result. In the path deformation from C to C_b shown in Figure 4, the residue of the intercepted pole must be accounted for, leading to the current representation

$$i_n = i_n^\infty + i_n^d, \qquad n \geq 0, \tag{19}$$

where, recalling (14),

$$i_n^\infty = V \frac{z_\gamma^n}{K(z_\gamma)} = V \frac{e^{-jk_{x0}nd}}{K(z_\gamma)}, \tag{20}$$

arises from the residue and the remaining contribution

$$i_n^d = \frac{V}{2\pi j} \frac{1}{K^-(z_\gamma)} \int_{C_b} \frac{1}{K^+(z)} \frac{z^n}{z - z_\gamma} dz \tag{21}$$

arises from the integration path C_b. (An analogous treatment could be carried out in the k_x domain, Figure 5.) The current representation (19) has a clear physical interpretation. The current contribution i_n^∞ represents the current that would exist on the infinite periodic array, while i_n^d is a correction contribution accounting for array-truncation effects. Indeed, as it will be clear in the following, i_n^d decreases away from the array truncation, and can be neglected sufficiently far from the truncation. It will be clear from its asymptotic evaluation that i_n^d behaves similarly to the field diffracted at the edge of a conducting semi-infinite half plane, and can therefore be interpreted as current diffracted at the truncation of the array.

[23] The diffracted current integral in (21) around the branch cut (see Figure 4) can be evaluated by direct integration on the z plane, or by using the change of variable

$$\sqrt{js} = \sqrt{kd - j \ln z}, \quad z = z_b e^{-s^2}, \tag{22}$$

with differential $dz = -2z_b\, s\, e^{-s^2}\, ds$. When z ranges from 0 to z_b and then again to 0 on the other side of the branch cut, as in Figure 4, the s variable ranges from $-\infty$ to 0 and then from 0 to ∞; thus (21) becomes

$$i_n^d = \frac{V}{\pi j} \frac{z_b^{n+1}}{K^-(z_\gamma)} \int_{-\infty}^{\infty} \frac{1}{K^+(z_b e^{-s^2})} \frac{s\, e^{-(n+1)s^2}}{z_b e^{-s^2} - z_\gamma} ds. \tag{23}$$

This integral representation is particularly suitable for numerical integration because it is on the steepest descent path and therefore it decays rapidly as $\exp(-s^2)$ away from the saddle point value at $s = 0$. The integrand also possesses poles at $s = \pm s_p$, with $s_p^2 \equiv j(k - k_{xp})$, that may occur close to or at the saddle point $s = 0$; i.e., when z_γ occurs close to or at z_b. This happens when a Floquet wave number k_{xp} along x matches the ambient wave number ($k_{xp} = k$), i.e., when one FW propagates grazing toward the positive x axis. In the work of *Hills and Karp* [1965] this condition was called inward resonance and certain aspects are treated by *Hills* [1965]. The outward resonance condition [*Hills and Karp*, 1965] occurs when a Floquet with wave number k_{xp} travels along $-x$ and matches $-k$; i.e., when $k_{xp} = -k$ for some p. Note that only the inward resonance condition implies that the pole is close to the saddle point and thus a different behavior (sometimes denoted as "transitional") of the diffracted current. The outward resonance condition only implies that the diffracted current i_n^d, as well as the infinite array term i_n^∞, grows in amplitude, because of the term $1/K^-(z_\gamma)$ in front of the integral in (21) or (31). To avoid numerical difficulties associated to the presence of a singularity near the integration path in (23), one can sum and subtract the regularizing function $Q(s)$ as for the Van der Waerden procedure discussed in section 6.2. The

regularized part is evaluated numerically with a few sampling points, while the remaining one is evaluated analytically providing the second term in brackets in (34).

5. Factorization of the Impedance $K(z)$

[24] In the previous section the impedance function $K(z)$ is factorized in (15) as the product of two functions, one regular outside and on the unit circle, $K^+(z)$, and the other regular inside and on the unit circle, $K^-(z)$. The factorization procedure plays a crucial role, especially when one desires an efficient numerical evaluation. In Appendix B we show a general method to factorize $K(z)$. When using the same basis and test functions $e(x) = h(x)$, one has that $K(z) = K(1/z)$ as for the rest of this paper. The factorization is rendered unique by imposing that $K^-(z) = K^+(1/z)$ and thus $K^-(0) = K^+(\infty) = k_0^+$. Here, we focus on an effective approximate closed form factorization, and how this is useful to simplify the numerical calculation of an exact factorization.

[25] For many engineering applications it may be convenient to approximate $K(z)$ by the simple expression

$$K(z) \approx K_{apr}(z) = K^+_{apr}(z)K^-_{apr}(z) \tag{24}$$

with

$$K^+_{apr}(z) = A\left(\frac{B}{\sqrt{1 - z_b/z}} + C\right), \tag{25}$$

$$K^-_{apr}(z) = K^+_{apr}\left(\frac{1}{z}\right) = A\left(\frac{B}{\sqrt{1 - z_b z}} + C\right). \tag{26}$$

and

$$A = \left(\frac{B}{\sqrt{1 - z_b^2}} + C\right)^{-1/2},$$

$$B = \frac{\zeta}{2}\sqrt{\frac{jk}{2d}}H(k)E^*\left(k^*\right), \tag{27}$$

$$C = \frac{jk\zeta}{4}\sum_{\substack{p=-\infty \\ p\neq 0}}^{\infty}\frac{H(k + 2\pi p/d)E^*\left(k^* + 2\pi p/d\right)}{\sqrt{-j\pi p}\sqrt{j(kd + \pi p)}}.$$

The original $K(z)$ is well approximated by $K_{apr}(z)$ in the neighborhood of the two branches. Indeed, when $z \to z_b$, one has $K(z) - K_{apr}(z) = O(\sqrt{z - z_b})$ and $K(z)/K_{apr}(z) \to 1$ because of the proper choice of the constants A, B, and C. Analogous properties are valid when $z \to 1/z_b$. Expression $K_{apr}(z)$ in (24) is readily factorized by inspection. The approximate $K_{apr}(z)$ and its factorization can be used in place of its exact expression in the current solution (18) or to efficiently evaluate the exact factorization (15). Indeed, we extract from $K^+(z)$ and $K^-(z)$ the approximate forms as

$$K^+(z) = K^+_{apr}(z)K^+_{res}(z) \tag{28}$$

$$K^-(z) = K^-_{apr}(z)K^-_{res}(z) \tag{29}$$

where $K^+_{res}(z)$ and $K^-_{res}(z)$ are unknown residual kernel functions smoother than $K^+(z)$ and $K^-(z)$ since we have extracted the dominant singularities at $z = z_b$ and $z = z_b^{-1}$. However, $K_{res}(z) \equiv K(z)/K_{apr}(z) = K^+_{res}(z)K^-_{res}(z)$ still has branches of higher order inside and outside the unit circle and its factorization is evaluated analogously to (B2) using

$$K^+_{res}(z) = \exp\left[\frac{1}{2\pi j}\oint_C \frac{\frac{1}{2}\left(1 + \frac{z}{s}\right)\ln K_{res}(s) - \ln K_{res}(z)}{s - z}ds\right]. \tag{30}$$

The numerical integration in (30) is easier to perform than that in (B2). Indeed, along the integration path, the integrand in (30) is limited also at the branch points of $K(s)$, $s = z_b$ and $s = z_b^{-1}$, where conversely the integrand in (B2) is singular. Moreover, in many practical cases the correction terms $K^+_{res}(z)$ and $K^-_{res}(z)$ may be approximated with a constant which does not affect the solution when (21) is rearranged in the way described after (18), i.e., by exploiting the fact that $K^+(z_\gamma)/K^+(z) \simeq K^+_{apr}(z_\gamma)/K^+_{apr}(z)$.

[26] The following numerical example shall explain and show the effectiveness of our approximate factorization. An array with period $d = 0.6\lambda$ and strip width $w = 0.1\lambda$ is considered. The basis $h(x)$ and test $e(x)$ functions are chosen as $h(x) = e(x) = 1/\left[\pi\sqrt{x(w - x)}\right]$ for $0 < x < w$ and 0 otherwise, such that they have built in the physical square root singularity at the strips edges. Their spectral counterparts are $H(k_x) = E(k_x) = J_0(k_x w/2)$, were J_0 is the Bessel function of zeroth order, that evaluated for $k_x = 0$ provides $H(0) = E(0) = 1$. The factor term $K^+(z)$ numerically evaluated via (B2), and the closed form approximate result $K^+_{apr}(z)$ in (25) are shown in Figures 6a and 6b, respectively. The thick (blue) and thin (red) lines are contour plots of the real and imaginary parts, respectively. Note in Figures 6a and 6b the branch point singularity at z_b and the relevant cut. It is clearly seen that $K^+(z) \approx K^+_{apr}(z)$ everywhere in the complex z plane. The ratio $K^+_{res}(z)$ between the $K^+(z)$ and $K^+_{apr}(z)$ is plotted in Figure 6c and is found to be almost unitary all over the complex z plane, especially onto the unit circle. Also note that all $K^+(z)$, $K^+_{apr}(z)$ and $K^+_{res}(z)$ exhibit a branch cut inside the unit circle from z_b to 0; however, $K^+(z)$ and $K^+_{apr}(z)$ are singular at the branch point z_b, whereas $K^+_{res}(z)$ is not. In Figure 7a the

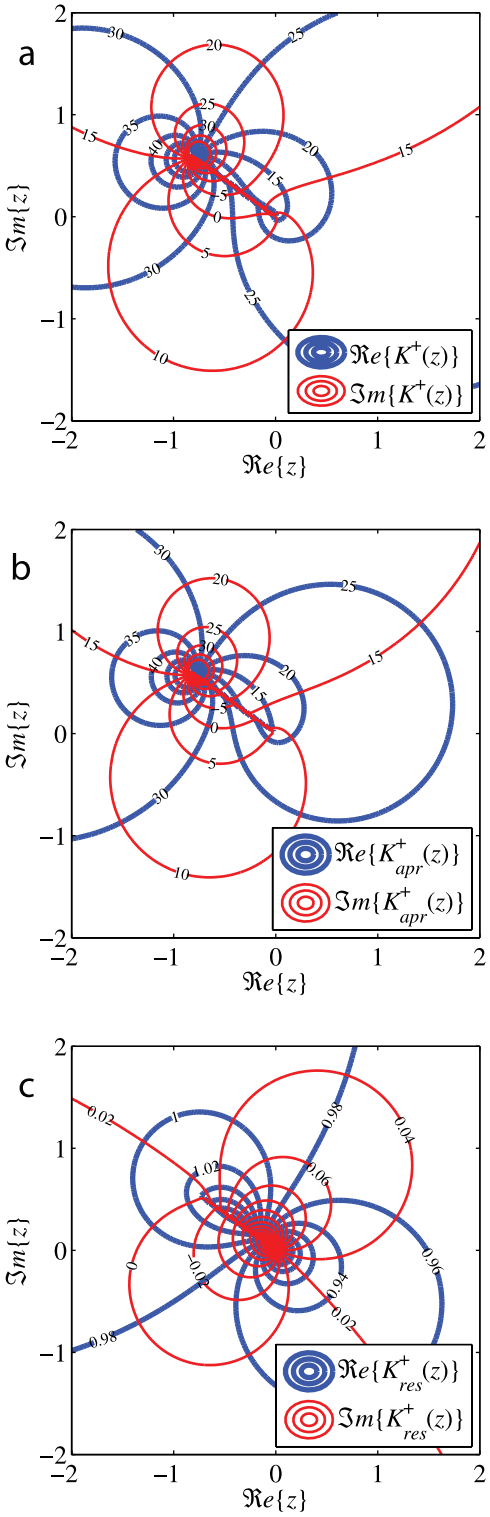

two factors $K^+(z)$ (continuous line) and $K^+_{apr}(z)$ (dashed line) are plotted along the unit circle, represented by the polar coordinate φ ranging from 0 to 2π. Both $K^+(z)$ and $K^+_{apr}(z)$ have the same singularity and phase jump at the branch point z_b. Clearly, $K^+_{apr}(z)$ well approximates $K^+(z)$ on the unit circle C. Note the singularity and the $\pi/2$ phase discontinuity. To emphasize that accuracy of the proposed approximate factorization is not limited to this particular example, the residual factor $K^+_{res}(z)$ is plotted in Figure 7b along the unit circle for various ratios of strip width and wavelength w/λ. In all cases it is not singular, its amplitude is almost equal to unity, and its phase is almost constant.

6. Asymptotic Approximation for Currents Far From the Truncation

[27] The diffracted currents i^d_n, $n = 0, 1, 2,..$ are here asymptotically evaluated for large n. It will be shown in the numerical examples in section 8 that this approximation is rather accurate also for small n. The integral in (21) around the branch cut (see Figure 4) is evaluated as in (23). That integral has a saddle point at $s = 0$ ($z = z_b$), and a double zero at $s = 0$, as can be seen by expanding $sK^+_{apr}(e^{-s^2}z_b) \approx -jAB$ for $s \approx 0$, which leads to

$$i^d_n \sim \frac{V}{\pi}\frac{z_b^{n+1}}{K^-(z_\gamma)}\frac{1}{AB}\int_{-\infty}^{\infty}\frac{s^2\, e^{-(n+1)s^2}}{z_b e^{-s^2} - z_\gamma}\, ds. \qquad (31)$$

Expression (31) will be evaluated in a nonuniform and a uniform fashions in the sequel. The steps are pretty similar to those in the work of *Capolino et al.* [2000a] and are here only summarized for space limitation.

6.1. Nonuniform Evaluation of the Diffracted Currents

[28] The nonuniform asymptotic evaluation of (31) is carried out evaluating at $s = 0$ the slowly varying part of the integrand, leading to

$$i^d_n \sim \frac{e^{-jk(n+1)d}}{(n+1)^{3/2}}\frac{D^d(k_{x0})}{z_b - z_\gamma}, \qquad (32)$$

where

$$D^d(k_{x0}) = \frac{-V}{2\sqrt{\pi}ABK^-(z_\gamma)}. \qquad (33)$$

Figure 6. Comparison between (a) $K^+(z)$ and (b) the closed form approximate result $K_{apr}{}^+(z)$, for a semi-infinite array with $d = 0.6\lambda$ and $w = 0.1\lambda$. Thick (blue, on line) and thin (red, on line) lines are contour plots of real and imaginary parts, respectively. Note that $K^+(z) \approx K_{apr}{}^+(z)$ everywhere. (c) $K_{res}{}^+(z) \approx 1$.

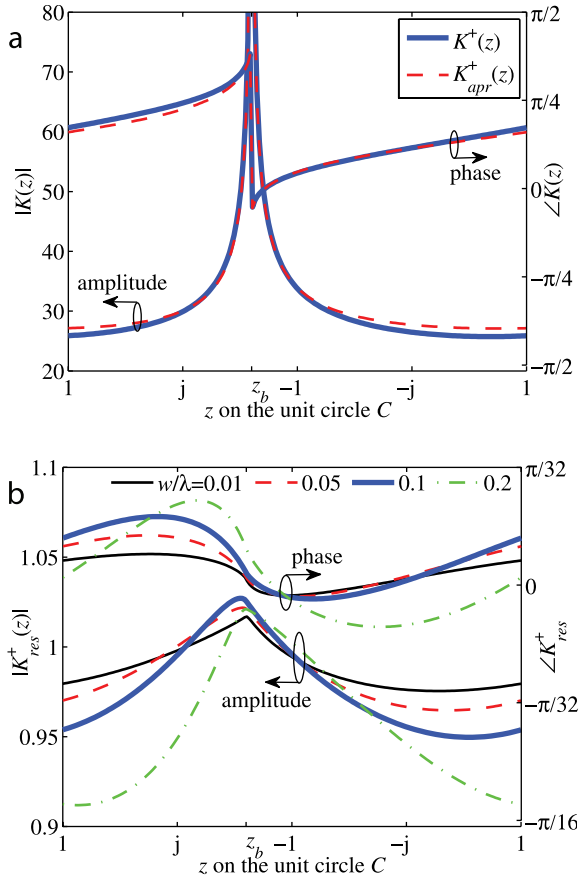

Figure 7. (a) Comparison between $K^+(z)$ (continuous line), and the closed form approximate result $K_{apr}{}^+(z)$ (dashed line), for z running on the unit circle C. $K_{apr}{}^+(z)$ well approximates $K^+(z)$. (b) Their ratio $K_{res}{}^+(z)$ is also plotted for various ratios of strip width and wavelength w/λ; in all cases it exhibits a small deviation from unity on the unit circle.

Note that the current asymptotically decays as $1/(n+1)^{3/2}$ away from the array truncation. The nonuniform evaluation diverges as a pole singularity when $z_\gamma \approx z_b$, that occurs when $k_{x,p} = k$ for some p. This is denoted as the inward resonance case that corresponds to the pth Floquet harmonic propagating at grazing angle $\phi = 0°$ causing a phase matching between the harmonic and the free space wave number. This mathematical nonphysical singularity is avoided when the asymptotic evaluation is performed in a uniform fashion as follows. Despite the current is not singular, the outward resonance is a peculiar condition that will be discussed also in section 8.3.

6.2. Uniform Evaluation of the Diffracted Currents

[29] The uniform evaluation is carried out performing the asymptotic evaluation uniformly with respect to the poles at $s = \pm s_p, p = 0, \pm 1, \ldots$, where $s_p^2 \equiv \ln(z_b/z_\gamma) + 2\pi jp = j(k_{xp} - k)d$. Therefore, when $z_b \approx z_\gamma$, two of the $\pm s_p$ poles approach the saddle point at $s = 0$. This peculiar condition happens when $k_{xp} = k$ for some p (inward resonance condition). The asymptotic evaluation is performed using a Van der Waerden regularization of the nearest $2P + 1$ poles to the saddle point, summing and subtracting the regularizing function $Q(s) = \sum_{p=-P}^{P} R_p s^2/(s^2 - s_p^2)$, where R_p is the residue of the integrand at the s_p pole, similarly to what was done by *Capolino et al.* [2000a]. In general one may want to extract more than the pair of nearest poles to $s = 0$ to render the integrand smoother and the asymptotics more accurate even for strip currents near the array truncation (small n). This leads to

$$i_n^d \sim \frac{e^{-jk(n+1)d}}{(n+1)^{3/2}} D^d(k_{x0}) \left[\frac{1}{z_b - z_\gamma} + \sum_{p=-P}^{P} \frac{1 - F_s\left(\delta_p^2\right)}{j(k - k_{xp})d} \right]. \tag{34}$$

where

$$F_s(x) = 2jx[1 - F(x)] \tag{35}$$

denotes the UTD "slope" Fresnel function, expressed in terms of the UTD Fresnel function of [*Kouyoumjian and Pathak*, 1974]

$$F(x) = 2j\sqrt{x}e^{jx} \int_{\sqrt{x}}^{\infty} e^{-t^2} dt, \tag{36}$$

whose argument is $\delta_p^2 = j(n+1)s_p^2 = (n+1)(k - k_{xp})d$. If one approximates $K^-(z_\gamma) \approx K(z_\gamma)/K^+_{apr}(z_\gamma)$, then (31) and (34) becomes closed form expressions that do not require any integration in the z domain.

[30] Note that when the argument $x \equiv \delta_p^2$ is large one has $F(x) \approx 1 - 1/(2jx) - 3/(4x^2) \approx 1$, and thus $1 - F_s(x) \approx 3/(2jx)$. Under this condition the leading term of the uniform evaluation (34) recovers the nonuniform one in (32). In other words, for the cases such that $\delta_p^2 \gg 1$ one has that i_n^d is predicted by (32) and decays as $1/(n+1)^{3/2}$. This condition does not happen when $k_{xp} \approx k$ which renders $x \equiv \delta_p^2 \approx 0$. In this case $F(x) \approx \sqrt{j\pi x}$ and thus $F_s(x) \approx 2jx$ which regularizes the zero $j(k - k_{xp})d$ at the denominator of (34). After noticing that the singular terms in the brackets $(z_b - z_\gamma)^{-1} + (j(k - k_{xp})d)^{-1}$ cancel out, one

has that the leading term in brackets is $[-2(n+1)]$, and thus i_n^d decays as $i_n^d \propto (n+1)^{-1/2}$, for all n such that $\delta_p^2 \ll 1$.

7. Evaluation of Currents Near the Truncation

[31] Near the truncation of the array, for small nkd, the asymptotic formula (34) is not accurate. One may use the standard numerical evaluation (21) with factorization (25), (26), to evaluate the currents on the first strips $n = 0, 1, 2\ldots$ near the truncation. Here we develop a simple and accurate method to evaluate i_0 and i_1 in closed form. We start from the expression of the total current i_n in (18). Note that the integrand has a branch point singularity at $z = z_b$, a simple pole at $z = z_\gamma$, both inside the unit circle (we recall that $K^+(z)$ is free of zeros and singularities outside the unit circle), and a pole singularity of order n at $z = \infty$. Here, (18) is evaluated for $n = 0$ by its residue at $z = \infty$. This is obtained using the change of variable $v = 1/z$, and evaluating the residue at $v = 0$, that leads to

$$i_0 = V \frac{1}{K^-(z_\gamma)K^+(\infty)}. \tag{37}$$

Analogously, after a few algebraic steps we can write that

$$i_1 = (z_\gamma + z_d) i_0. \tag{38}$$

with $z_d \equiv K^+(\infty)g^{(1)}(0)$, where $g^{(1)}$ is the first derivative of $g(v) = [K^+(1/v)]^{-1}$. Therefore we can write $z_d = \lim_{v\to 0}[1 - K^+(1/v)/K^+(\infty)]/v$, which is performed numerically in the next numerical examples. We recall that for the chosen factorization we have $K^+(\infty) = K^-(0)$. From a comparison between the total current i_0 on the first strip at the of a semi-infinite array (37) and the infinite array current i_0^∞ in (20), one obtains the interesting relation $i_0/i_0^\infty = K^+(z_\gamma)/K^+(\infty)$.

[32] The diffracted current on the first two strips $n = 0$, 1 is obtained by $i_n^d \equiv i_n - i_n^\infty$, where i_n^∞ is the current on the infinite array (20). Formulas similar to (37) and (38) are easily derived for any i_n involving nth derivatives that, however, are complicated for $n > 1$.

8. Illustrative Examples: Current on the Truncated Array

[33] In the next illustrative examples we compare the Wiener-Hopf solution with a method of moments (MOM) constructed with a single basis function $h(x)$ on 1000 conducting strips. In this way the two methods have the same basis $h(x)$ and test $e(x)$ functions, and the comparison is only for analyzing the Wiener-Hopf behavior of the solution. The factorization is performed numerically via (30) with (28) and (25) by summing several integrand samples uniformly distributed on the unit circle C. As discussed in the text, this is numerically advantageous compared to (B1) or (B2) because the integrand in (30) is regular. The current i_n on the strips is evaluated numerically using (19) with (20) and (23). The diffracted current i_n^d in (23) is evaluated numerically by summing integrand samples distributed from $s = -6$ to $s = 6$. In the following examples we also test the uniform asymptotic evaluation (34). Away from the truncation, the diffracted current decays asymptotically as $i_n^d \propto (n+1)^{-3/2}$ in almost all cases, except for the transverse inward resonant case ($k_{xp} \approx k$) and except for the low-frequency case. For comparison we also report the current i_n^∞, (20), on the infinite array.

8.1. Comparisons: Exact, Asymptotics, MoM

[34] In Figure 8 the current i_n on the conducting strips is shown for the three different incidence angles $\phi' = 60°$, 90°, 120°. The strips period is $d = 0.6\lambda$, and the strips width is $w = 0.1\lambda$. The agreement between the Wiener-Hopf (WH, pluses) and the MoM (crosses) solutions is excellent, and the current away from the truncation tends to the current on the infinite array i_n^∞ (dashed line). The asymptotic solution (continuous line with dots) accurately predicts the current for $n \geq 3$, but the exact value of this n for which we have accuracy depends on the incidence angle ϕ' and on the normalized period d/λ.

8.2. Low- and High-Frequency Behavior

[35] We show here that the Wiener-Hopf solution is accurate also for the low-frequency ($d \ll \lambda$) and high-frequency ($d \gg \lambda$) cases. For example, in Figure 9 the period is $d = 0.04\lambda$, and $w = 0.01\lambda$. In Figure 10 the period is $d = 9.7\lambda$ and strip width $w = 0.1\lambda$, thus w is still much smaller than the wavelength so as the single basis function approximation is still justifiable. The Wiener-Hopf solution is in good agreement with the MoM solution in both cases. The asymptotic solution also accurately predicts the current. Note that for the low-frequency case the truncation effects extend on a large portion of the array, because the asymptoticity of the solution is achieved only for large n. Note that the "slope" Fresnel function $F_s(\delta_p^2)$ approaches unit for large argument δ_p^2, which is large for large n. The diffracted current i_n^d extends on a large portion when it is in "transition," which is defined by a nonlarge argument δ_p^2. This behavior is discussed with more details by *Capolino et al.* [2000a, 2000b]. For the high-frequency case (large period) the total current i_n in (18) tends immediately to the current of the infinite array $i_n\infty$ because while the truncation-induced diffracted current propagates toward large ns it radiates (some of its Floquet harmonics is in the visible region $-k < k_{xp} < k$) and so it rapidly attenuates.

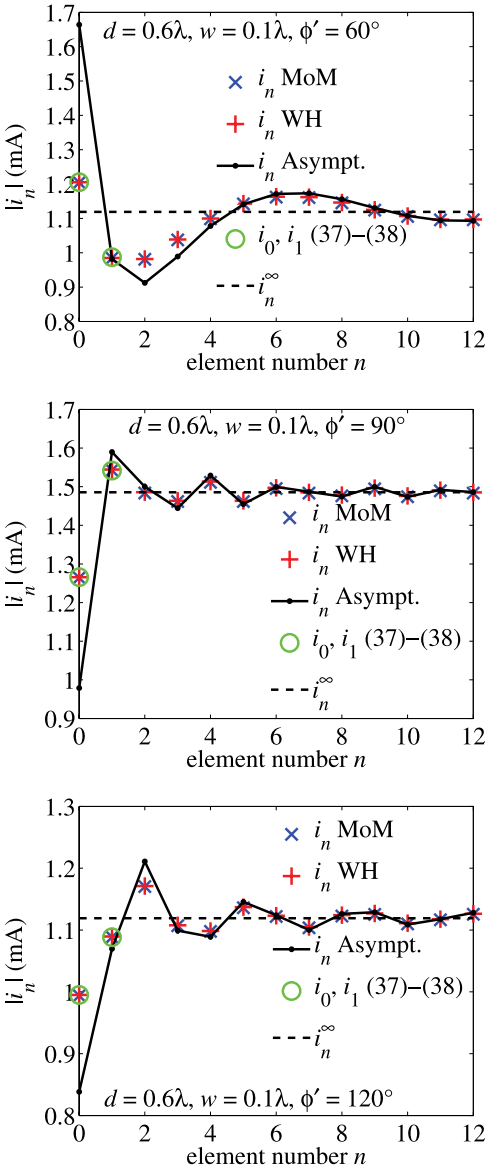

Figure 8. Current i_n versus strip element number n. Comparison between the Wiener-Hopf result (18) with (28) and (30) (pluses), and the MoM (crosses). Also shown is the asymptotics in (34) (continuous line with dots), and the simplified formula for i_0 and i_1 in (37) (open circles). The strip width is $w = 0.1\lambda$, and the array period is $d = 0.6\lambda$. Currents are evaluated for three incidence angles: $\phi' = 60°$, $90°$, $120°$.

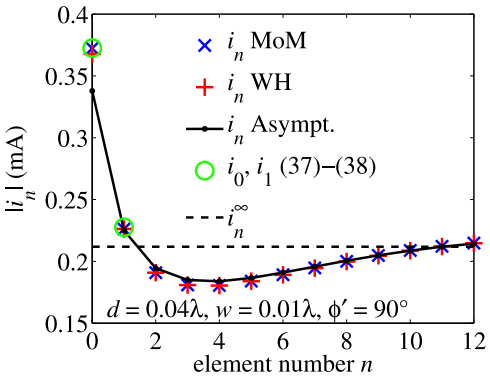

Figure 9. Current versus strip element number for the low-frequency case. The period is $d = 0.04\lambda$.

8.3. Inward and Outward Resonant Cases

[36] Here we analyze the particular cases of inward or outward resonances, that occur when $k_{xp} = k$ or $k_{xp} = -k$, respectively. In other words when $z_\gamma = z_b$ or $z_\gamma = 1/z_b$, respectively. For instance, suppose that the strip grating is illuminated by a plane wave coming from a direction ϕ' (Figure 1) and that the grating period $d > \lambda/2$, therefore the the inward and outward cases may correspond to $k_{x,1} = k$ and $k_{x,-1} = -k$, respectively. These conditions are verified when $\cos\phi' = \lambda/d - 1$ (inward resonance) and when $\cos\phi' = -(\lambda/d - 1)$ (outward resonance). In our particular case with period $d = 0.6\lambda$ (an width $w = 0.1\lambda$) the conditions are met when $\phi' = 48.2°$ (inward resonance) and for $\phi' = 131.8°$ (outward resonance). In Figure 11 we show the current for $\phi' = 131°$, very close to the outward resonance condition. The main effect of this condition is to have i_n^∞ and i_n, and so as i_n^d, to be smaller than the other cases because of the growing of the $K^-(z_\gamma)$ function at the denominators of (18) and (20).

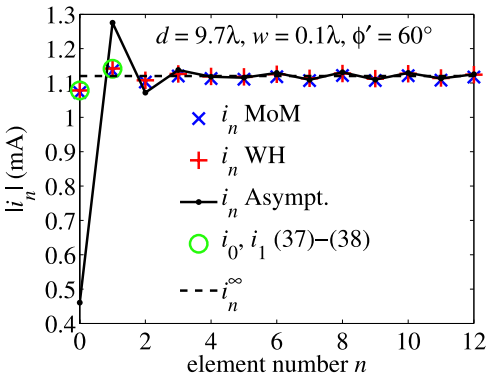

Figure 10. Current versus strip element number for the high-frequency case. The period is $d = 9.7\lambda$.

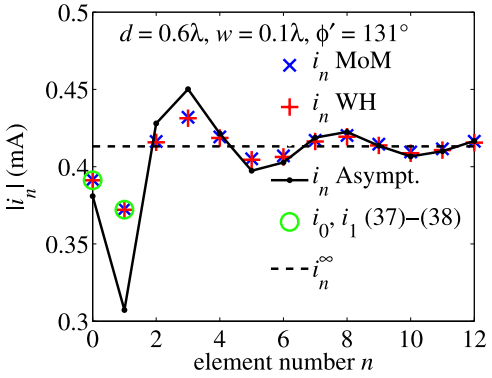

Figure 11. Current versus strip element number for $\phi' = 131°$ close to the outward resonant case $k_{x,-1} \approx -k$.

[37] In Figure 12 we show the current i_n for $\phi' = 48°$, very close to the inward resonance condition. Note that the diffracted current has a different effect compared to the previous nonresonant cases or to the outward resonant case. The current variation with respect to the infinite array solution is stronger and extends on a large portion of the array. As already anticipated in section 6, for the inward resonance case one has a small δ_p because $k_{x,1} \approx k$, unless n is very large, and this causes the Fresnel function in (34) to vanish. Under this condition the current decay changes from $(n + 1)^{-3/2}$. It decays slower than this until a large value of n renders δ_p large anyway. More details about asymptotic transitions are given by *Capolino et al.* [2000b].

8.4. Array-Current Trends: Nontransitional and Transitional Diffraction

[38] In Figure 13 we show the trend of the diffracted current $i_n^d = i_n - i_n^\infty$ for various incidence angles ϕ', for an array with period $d/\lambda = 0.6$. We have included

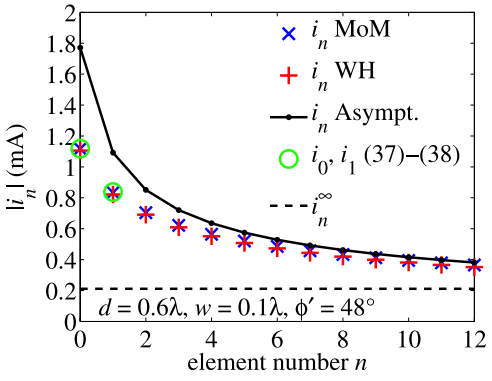

Figure 12. Current versus strip element number for $\phi' = 48°$ close to the inward resonant case $k_{x,1} \approx k$.

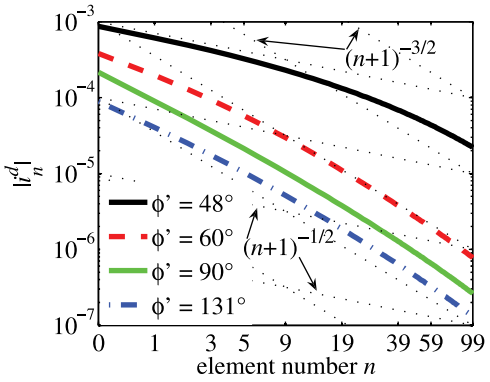

Figure 13. Asymptotic trend of current i_n^d versus strip number n for various incidence angles. Note that asymptotically, far from the truncation, the current decays as $i_n^d \propto (n + 1)^{-3/2}$ for all cases, though this happens for large n when approaching the inward resonance case $\phi' = 48.2°$.

incidence angles close to the inward $\phi' = 48.2°$ and outward $\phi' = 131.8°$ resonance cases.

[39] For all cases, except for the inward resonance case, the trend $i_n^d \sim (n + 1)^{-3/2}$ occurs starting from small n. From the asymptotic solution, valid for large n, we note that the decay eventually is $i_n^d \sim (n + 1)^{-3/2}$, as predicted from the nonuniform evaluation in (32). As said in section 6 the uniform and nonuniform evaluations in (34) and (32) coincide for large δ_p, which is achieved for moderate and large n when $k_{xp} \neq k$. For the inward resonance case in Figure 13, this $i_n^d \sim (n + 1)^{-3/2}$ decay occurs only when $n > 60$. This is explained by noticing that for the inward resonance case $k_{xp} \approx k$ and thus large δ_p is obtained only at larger values of n compared to the other nonresonant cases.

9. Conclusion

[40] We have presented a novel formulation to analyze the behavior of the current induced on truncated arrays of narrow strips. For the first time we have shown a clear relation between the standard k_x complex spectral plane and the less standard z domain spectral plane. The solution is easy to evaluate, also thanks to special techniques to regularize the factorization and current integrals shown in this paper for the first time. Uniform and nonuniform asymptotic evaluations have been carried out, establishing clearly the $i_n^d \sim (n + 1)^{-3/2}$ general trend of the diffracted current away form the truncation, valid in most cases, and always in the case of very large n. The special cases of inward and outward resonances have also been treated and discussed. We believe that this paper is useful to clarify several issues related to trun-

cated arrays since most of the properties shown can be generalized to more complicated elements (not shown here) that, however, cannot be treated via this simple discrete Wiener-Hopf method. Currents on the simple truncated array in this paper are treated and modeled rigorously.

Appendix A: *Z* Transform

[41] The bilateral Z transform of the samples k_n is defined as

$$K(z) = \sum_{n=-\infty}^{\infty} k_n z^{-n} \tag{A1}$$

and its inverse by

$$k_n = \frac{1}{2\pi j} \int_C K(z) z^{n-1} dz. \tag{A2}$$

For a monolateral succession of samples k_n^+, such that $k_n^+ = 0$ for $n < 0$, the initial value theorem states that $K(z \to \infty) \to k_0^+$.

Appendix B: Factorization

[42] The product factorization $K(z) = K^+(z)K^-(z)$ in the z domain can be obtained using the representation $K(z) = \exp[\ln K(z)]$ and then applying the sum splitting $\ln K(z) = \ln K^+(z) + \ln K^-(z)$ (see *Noble* [1958] and *Kobayashi* [1990] for the same procedure in the k_x spectral plane), that leads to

$$K^+(z) = \exp\left(\frac{1}{2\pi j} \oint_{C_1} \frac{\ln K(z)}{z - s} ds\right). \tag{B1}$$

The integrand has a pole singularity at $s = z$, and C_1 is the unit circle properly deformed to leave outside the pole at $s = z$, if $|z| \leq 1$. An equivalent representation is obtained using the procedure shown in Appendix C (equation (C2)), leading to

$$K^+(z) = \exp\left(\frac{1}{2\pi j} \oint_C \frac{\frac{1}{2}\left(1 + \frac{z}{s}\right) \ln K(s) - \ln K(z)}{z - s} ds\right). \tag{B2}$$

The last expression furnishes the same function $K^+(z)$ but its integrand is smoother then that in (B1). It posses only the branch point singularities at $z = z_b$ and $z = 1/z_b$ of the function $K(s)$ because the pole singularity at $s = z$ is regularized. Furthermore the integration path is the unit circle with no need of deformation, thus simplifying its numerical evaluation. In this paper we choose that $e(x) = h(x)$ and thus $K(z) = K(1/z)$, as a consequence it is easy to verify that the sum splitting shown in Appendix C leads to the property $K(z) = K^+(z)K^+(1/z)$, i.e., $K^-(z) = K^+(1/z)$, and

$$K^+(\infty) = K^-(0) = k_0^+ = e^{\frac{1}{2\pi j} \oint_C \frac{\ln K(s)}{2s} ds}. \tag{B3}$$

Moreover, since either zeroes or poles of $K^+(z)$ are connected to singularities of the argument of the exponential function in (B2), $K^+(z)$ ($K^-(z)$) is found to be free of zeroes and singularities inside (outside) and on the unit circle.

[43] The factorization (B2) can now be evaluated performing a numerical integration along the unit circle. However, it is shown in the following that this numerical integration can be made more efficiently or completely avoided by resorting to an effective approximate closed form factorization.

Appendix C: Sum Splitting

[44] The splitting of a Z transform $F(z) = F^+(z) + F^-(z)$ (of a sequence f_n) as the sum of two functions F^+ and F^- is trivial. It is sufficient to split the infinite bilateral sequence f_n as the sum of two infinite monolateral sequences $f_n = f_n^+ + f_n^-$, with $f_n^+ = 0$ for $n < n^+$ and $f_n^- = 0$ for $n > n^-$, where n^+ and n^- are two arbitrary finite integers such that $n^+ \geq n^-$. Obviously this splitting is not unique. If the original sequence, as in our case, is symmetric ($f_n = f_{-n}$), and in turn its Z transform is such that $F(z) = F(1/z)$, one can impose the constraint $F^-(z) = F^+(1/z)$, i.e., that $f_n^- = f_{-n}^+$ (that also implies that $n^+ = -n^-$). Furthermore, imposing also that $n^- = n^+ = 0$, i.e., that f_n^+ (f_n^-) vanishes for negative (positive) n, or equivalently, through the initial value theorem, that $F^+(\infty)$ ($F^-(0)$) is a constant, one renders the splitting unique obtaining $f_n^+ = f_n u_n$, being u_n the unit step sequence defined by $u_n = 0, \frac{1}{2}, 1$ for $n<, =, >0$. As a consequence, the desired splitting of the function $F(z)$ is calculated via a convolution with the Z transform of u_n, as

$$F^+(z) = \frac{1}{2\pi j} \oint_{C_1} F(s) \frac{s + z}{s - z} \frac{ds}{2s} \tag{C1}$$

where C_1 is defined in Appendix B. It is easy to verify that, with the definition (C1), $F(z) = F^+(z) + F^+(1/z)$ and $F^+(\infty) = \frac{1}{2} f_0$ as required. In order to avoid the pole singularity in the integrand and the cumbersome definition of the integration path, (C1) is rearranged as

$$F^+(z) = \frac{1}{2\pi j} \oint_C \frac{\frac{1}{2}\left(1 + \frac{z}{s}\right) F(s) - F(z)}{s - z} ds \tag{C2}$$

where the integration path is chosen onto the unit circle and the integrand is analytically continued to its limit value $\frac{d}{dz} F(z) - \frac{1}{2z} F(z)$ at $s = z$. The representation (C2) is

more suitable for numerical evaluation running on a fixed path (whose definition does not depend on the value of z, as for C_1) that is free of singularities (except for those belonging to $F(s)$, if any).

[45] **Acknowledgments.** The authors would like to acknowledge useful discussions with A. Alkumru, M. Idemen, and C. Linton. Filippo Capolino also acknowledges inspirational contributions from Sabina Trzan.

References

Born, M., and E. Wolf (1965), *Principles of Optics*, 3rd ed., Oxford, U. K.

Capolino, F., M. Albani, S. Maci, and R. Tiberio (1998), High frequency analysis of an array of line sources on a truncated ground plane, *IEEE Trans. Antennas Propag.*, *46*(4), 570–578.

Capolino, F., M. Albani, S. Maci, and L. B. Felsen (2000a), Frequency domain Green's function for a planar periodic semi-infinite dipole array. Part I: Truncated Floquet wave formulation, *IEEE Trans. Antennas Propag.*, *48*(1), 67–74.

Capolino, F., M. Albani, S. Maci, and L. B. Felsen (2000b), Frequency domain Green's function for a planar periodic semi-infinite dipole array. Part II: Phenomenology of diffracted waves, *IEEE Trans. Antennas Propag.*, *48*(1), 75–85.

Carin, L., and L. Felsen (1993), Time harmonic and transient scattering by finite periodic flat strip arrays: Hybrid (ray)-(Floquet mode)-(MoM) algorithm, *IEEE Trans. Antennas Propag.*, *41*(4), 412–421.

Çivi, Ö. A., P. H. Pathak, H.-T. Chou, and P. Nepa (2000), A hybrid UTD-MoM for efficient analysis for radiation/scattering from large finite planar arrays, *Radio Sci.*, *35*(2), 607–620.

Craeye, C., A. G. Tijhuis, and D. H. Schaubert (2004), An efficient mom formulation for finite-by-infinite arrays of two-dimensional antennas arranged in a three-dimensional structure, *IEEE Trans. Antennas Propag.*, *52*, 271–282.

Fel'd, I. N. (1958), Diffraction of electromagnetic waves on a semi-infinite grating, *Radiotekh. Electron.*, *3*, 882–889.

Felsen, L., and L. Carin (1994), Frequency and time domain Bragg-modulated acoustics for truncated periodic arrays, *J. Acoust. Soc. Am.*, *95*(2), 638–649.

Hills, N. L. (1965), Semi-infinite diffraction gratings. II. Inward resonance, *Commun. Pure Appl. Math.*, *18*, 389–395.

Hills, N. L., and S. N. Karp (1965), Semi-infinite diffraction gratings - I, *Commun. Pure Appl. Math.*, *18*, 203–233.

Jones, D. S. (1964), *The Theory of Electromagnetism*, Pergamon, Oxford, U. K.

Kildal, P.-S. (1984), Diffraction corrections to the cylindrical wave radiated by a linear array feed of a cylindrical reflector antenna, *IEEE Trans. Antennas Propag.*, *32*, 1111–1116.

Kobayashi, K. (1990), Wiener-Hopf and modified residue calculus techniques, in *Analysis Methods for Electromagnetic Wave Problems*, edited by E. Yamashita, chap. 8, Artech House, Boston, Mass.

Koughnett, A. L. V. (1970), Mutual coupling effects in linear antenna arrays, *Can. J. Phys.*, *48*, 659–674.

Kouyoumjian, R. G., and P. H. Pathak (1974), A uniform geometrical theory of diffraction for an edge in a perfectly conducting surface, *Proc. IEEE*, *62*(11), 1448–1461.

Linton, C. M., and P. A. Martin (2004), Semi-infinite arrays of isotropic point-scatterers. a unified approach, *SIAM J. Appl. Math.*, *64*, 1035–1056.

Neto, A., S. Maci, G. Vecchi, and M. Sabbadini (2000a), Truncated Floquet wave diffraction method for the full wave analysis of large phased arrays. Part I: Basic principles and 2D case, *IEEE Trans. Antennas Propag.*, *48*(3), 594–600.

Neto, A., S. Maci, G. Vecchi, and M. Sabbadini (2000b), Truncated Floquet wave diffraction method for the full wave analysis of large phased arrays. Part II: Generalization to the 3D case, *IEEE Trans. Antennas Propag.*, *48*(3), 600–611.

Nishimoto, N., and H. Ikuno (1999), Analysis of electromagnetic wave diffraction by a semi-infinite strip grating and evaluation of end-effects, *Prog. Electromagn. Res.*, *23*, 39–58.

Noble, B. (1958), *Methods Based on the Wiener-Hopf Technique*, Pergamon, London.

Wasylkiwskyj, W. (1973), Mutual coupling effects in semi-infinite arrays, *IEEE Trans. Antennas Propag.*, *21*(3), 277–285.

Wasylkiwskyj, W., and W. Kahn (1970), Theory of mutual coupling among minimum-scattering antennas, *IEEE Trans. Antennas Propag.*, *18*(2), 204–216.

M. Albani, Department of Information Engineering, University of Siena, I-53100 Siena, Italy.

F. Capolino, Department of Electrical Engineering and Computer Science, University of California, Irvine, CA 92697, USA. (f.capolino@uci.edu)